



Article

# Punching Shear of FRP-RC Slab–Column Connections: A Comprehensive Database

Yazan Almomani <sup>1</sup>, Roaa Alawadi <sup>2</sup>, Ahmad Tarawneh <sup>3,\*</sup> , Abdullah Alghossoon <sup>3</sup> and Ahmad Aldiabat <sup>3</sup>

<sup>1</sup> Civil Engineering Department, Faculty of Engineering, University of Petra, Amman 11196, Jordan; yazan.almomani@uop.edu.jo

<sup>2</sup> Civil Engineering Department, Applied Science Private University, Amman 11937, Jordan; r\_alawadi@asu.edu.jo

<sup>3</sup> Civil Engineering Department, Faculty of Engineering, The Hashemite University, P.O. Box 330127, Zarqa 13133, Jordan; abduallahm\_ab@hu.edu.jo (A.A.); 2170518@std.hu.edu.jo (A.A.)

\* Correspondence: ahmadn@hu.edu.jo

**Abstract:** Several design standards have been developed in the last two decades to estimate the punching capacity of two-way reinforced concrete (RC) slabs reinforced with fiber-reinforced polymer (FRP) reinforcement. FRP-RC design standards include the recently published ACI 440.11-22, CSA/S806-12, and JSCE-2007. These models are either based on empirical data or semi-empirical methods and calibrated using different databases. Additionally, these standards do not have provisions for connections with shear reinforcement. Therefore, a reliable worldwide database for developing and assessing the applicability of such provisions with test results is vital. This study presents a worldwide and up-to-date database for punching shear of FRP-RC slabs. The database includes 197 tested connections, comprising interior and edge connections, with and without shear reinforcement, and a wide range of materials and cross-sectional properties. The database was used to evaluate the accuracy of the mentioned standards in predicting the punching shear capacity. For connections without shear reinforcement, it was determined that the three design standards yielded similar performance with different conservatism levels. ACI 440.11-22 yielded the most conservative results, with average  $V_{exp}/V_{pred}$  ratios of 2.04 compared to 1.28 and 1.3 for other models. For connection with shear reinforcement, specimens with  $E_{vf} > 100$  GPa resulted in  $V_{exp}/V_{pred}$  ratios less than 1.0 for ACI and CSA standards.

**Keywords:** FRP-RC slabs; punching shear; slab–column connection; code evaluation; database



**Citation:** Almomani, Y.; Alawadi, R.; Tarawneh, A.; Alghossoon, A.; Aldiabat, A. Punching Shear of FRP-RC Slab–Column Connections: A Comprehensive Database. *J. Compos. Sci.* **2024**, *8*, 145. <https://doi.org/10.3390/jcs8040145>

Academic Editors: Xiangfa Wu and Oksana Zhlobko

Received: 12 March 2024

Revised: 3 April 2024

Accepted: 10 April 2024

Published: 12 April 2024



**Copyright:** © 2024 by the authors. Licensee MDPI, Basel, Switzerland. This article is an open access article distributed under the terms and conditions of the Creative Commons Attribution (CC BY) license (<https://creativecommons.org/licenses/by/4.0/>).

## 1. Introduction

Due to reinforcing steel bar corrosion, the deterioration of reinforced concrete structures, buildings, and bridges is a major problem that shortens the service life of steel-reinforced concrete (RC) structures. Fiber-reinforced polymer (FRP) reinforcing bars have emerged as a cost-effective alternative to traditional steel bars due to their high corrosion resistance. Compared to conventional steel rebars, FRP bars exhibit superior tensile strength, demonstrating linear elastic behavior until failure without a yield plateau. Their elastic moduli are lower compared to steel, typically ranging from 20% to 80% of the elastic modulus of steel, depending on the type of fibers used [1]. FRP bars can be made of aligned fibers of glass (GFRP), carbon (CFRP), basalt (BFRP), or aramid (AFRP). Other advantageous properties of FRP bars are their high strength-to-weight ratio and non-magnetic properties. Several established design guidelines for FRP-RC members include ACI 440.11-22 [2], CSA/S806 [3], and JSCE [4]. The design of FRP-RC is continuously updated based on the research findings.

Punching shear in flat-plate FRP-RC slabs is a major concern that usually governs the design [5], where inclined shear cracks surface near columns to form a truncated pyramid-shaped failure surface, as illustrated in Figure 1. This phenomenon arises due to

the relatively small thickness of the slab and its direct support on columns, resulting in high shear stresses transferred between the slab and columns. Several experimental studies have shown that FRP-RC slabs exhibit a lower punching shear capacity than their steel-RC counterparts, even when having the same flexural reinforcement ratio. This discrepancy is attributed to the lower axial and transverse stiffness of FRP reinforcement compared to steel bars, leading to wider cracks, reduced aggregate interlock and dowel action resistance, and a shallower neutral axis depth [5,6]. Consequently, punching shear models in FRP design guidelines incorporate the elastic modulus as a variable. Additionally, when utilizing FRP bars as shear reinforcement to resist punching shear, it is important to note that the tensile strength of the bent portion is significantly lower than that of the straight portion. Therefore, the shear contribution provided by FRP shear reinforcement depends on the bent strength or the level of stresses attained in the shear reinforcement [7].

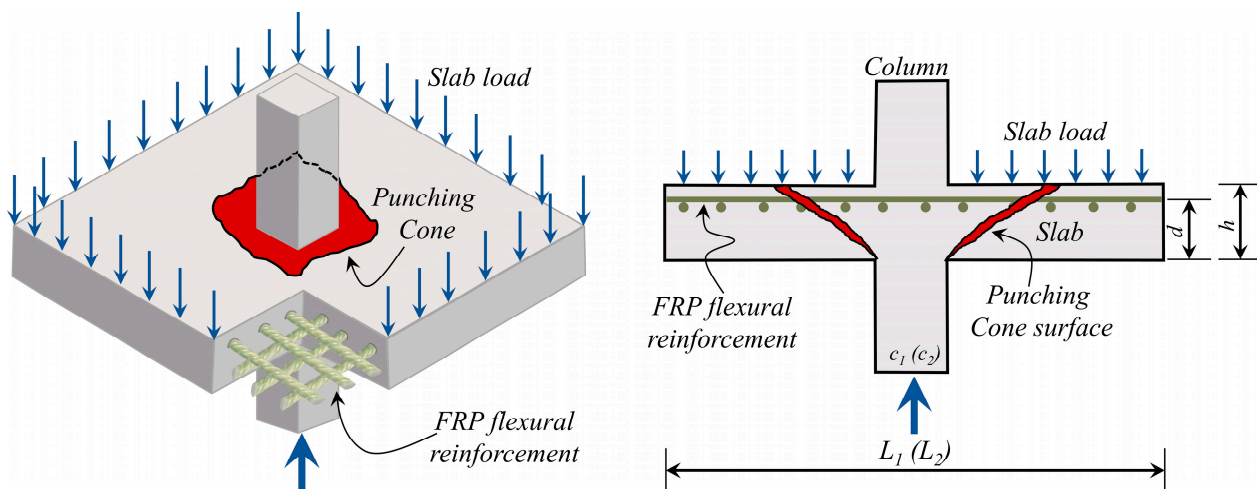


**Figure 1.** Punching shear failure in column–slab connection.

The adopted models for punching shear in FRP-RC slabs are empirically or semi-empirically calibrated with experimental data. The majority of the experimental data used in the calibration have been obtained before developing the models and focus on punching shear due to concentric loading [5]. Additionally, proposed models may not have been calibrated with the same database, which makes it inconvenient to compare models calibrated using different databases. In this study, an intensive literature review was conducted to create an up-to-date evaluation database for punching shear of FRP-RC slabs. The database includes interior and edge connections (i.e., concentric shear force and unbalanced bending moment), with and without shear reinforcement. The database is used to assess punching shear models adopted in design guidelines. The assessment is conducted based on statistical measures.

## 2. Concentric and Eccentric Punching Shear Behavior

As mentioned, punching shear failure starts with inclined cracks propagating from the tension to the compression side around the columns when the combined shear and flexural stress exceeds the concrete capacity, forming a truncated pyramid-shaped failure surface. In the case of an interior slab–column connection in braced frames, only shear stresses are transferred from slab to columns, and the negligible moment is transferred at the connection. The imposed stresses can be calculated as shown in Equation (1), where  $V_f$  is the factored shear force transferred between slab and column,  $d$  is the slab effective depth, and  $b_o$  is the perimeter of the critical section at a distance of  $d/2$  from column face. This

assumes a uniform stress distribution along the critical perimeter (Figure 2a). However, studies have indicated that stress at the corners of the critical section is higher [8].

$$v_c = \frac{V_f}{b_0 d} \tag{1}$$

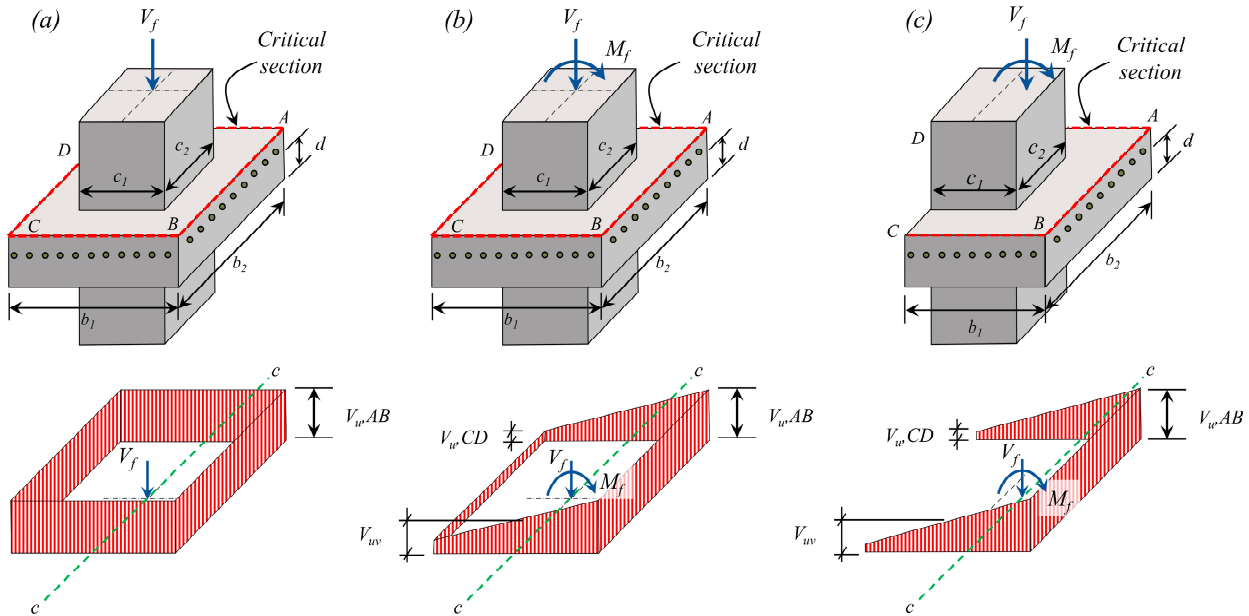


**Figure 2.** Shear stress distribution in (a) interior connection with concentric load, (b) interior connection with eccentric load, (c) edge connection with eccentric load.

When a lateral load or unbalanced moment causes a transfer of moment between the slab and column, a fraction of the unbalanced moment will be transferred by direct flexure ( $\gamma_f$ ), and the remaining will be transferred by shear ( $\gamma_v$ ), according to Equation (2) (where  $b_1$  is the width of the critical section in the direction of the unbalanced moment and  $b_2$  is the width of the critical section perpendicular to  $b_1$ ). Accordingly, the maximum shear stress can be computed by adding the shear stresses due to direct shear (Equation (1)) and the shear stresses due to the moment transfer about the centroid of the critical section in Equation (3) (Figure 2b,c), where  $M_f$  represents the factored moment transferred between the slab and column,  $J_c$  denotes a property of the critical section similar to the polar moment of inertia, and  $e$  represents the distance from the centroid of the critical shear section to the point where shear stress is being calculated. This shear stress model is adopted in both ACI 318-19, ACI 440.11-22, and CSA/A23.3-19 [5]. However, the JSCE provisions include the effect of eccentric loading by a factor ( $1/\alpha$ ), as will be shown in the next section. Typically, connections between slabs and columns positioned at corners and edges experience moment transfer and eccentric loading. However, these scenarios have received less attention in research compared to internal slab–column connections subjected to concentric loads [9].

$$\gamma_v = 1 - \frac{1}{1 + (2/3)\sqrt{b_1/b_2}} \tag{2}$$

$$v_c = \frac{V_f}{b_0 d} + \frac{\gamma_v M_f e}{J_c} \tag{3}$$

The current design codes do not include provisions for including the contribution of shear reinforcement in punching shear. However, by following the design provisions for steel-RC two-way shear, the resistance of the slab can be computed by combining the concrete resistance ( $V_c$ ) and the shear reinforcement resistance ( $V_f$ ) if it exists, according to Equations (4) and (5), where  $A_{vf}$ ,  $f_{fv}$ , and  $s$  are the total shear reinforcement area, the

stress in shear reinforcement, and the spacing of shear reinforcement, respectively. The ACI 440 and CSA/S806 limit the stress in shear reinforcement (for one-way shear) to  $0.005 E_f$  ( $E_f$  = elastic modulus of FRP shear reinforcement).

$$V_n = V_c + V_f \quad (4)$$

$$V_f = \frac{A_{vf} f_f v d}{s} \quad (5)$$

### 3. Code Provisions

Punching shear design models for FRP-RC slabs typically adapt existing models designed for steel-RC slabs to accommodate the notable differences between FRP and steel, particularly focusing on variations in axial stiffness. This section reviews the FRP-RC punching shear models adopted in ACI 440.11-22, CSA/S806-12, and JSCE 1997.

#### 3.1. Punching Shear Model Adopted in ACI 440.11-22

In 2005, Ospina, through statistical analysis, demonstrated that the one-way shear model initially proposed by Tureyen and Forsch in 2003 [10] could be adapted to address shear transfer in two-way concrete slabs [11]. This adaptation resulted in Equations (6a)–(6e), which are utilized for computing concentric punching shear. Presently, this model is integrated into ACI 440.11-22 [2]. It is worth noting that Equation (6a) corresponds to the fundamental punching shear model outlined in ACI 318 for steel-reinforced concrete (RC) slabs, but multiplied by a factor of  $2.5 k_{cr}$  to consider the axial stiffness of fiber-reinforced polymer (FRP) reinforcement. The parameter  $k_{cr}$  represents the ratio of the elastic neutral axis depth to the depth of longitudinal reinforcement and can be determined for slabs using the equation provided for rectangular sections in Equation (6b). Furthermore, the model incorporates the size effect ( $\lambda_s$ ) as depicted in Equation (6e). In Equations (6a)–(6e),  $f'_c$ ,  $b_o$ ,  $d$ ,  $N_c$ , and  $\rho$  denote the concrete compressive strength, perimeter of the critical section at a distance of  $d/2$ , effective depth, modular ratio, and average tensile longitudinal reinforcement ratio, respectively.

Research has indicated that Equation (6a) of the shear model could underestimate shear capacity significantly for lightly reinforced concrete elements like slabs. Consequently, a lower limit (Equation (6d)) is prescribed accordingly (Nanni et al., 2014) [12].

$$V_c = 0.8 \lambda_s \sqrt{f'_c} k_{cr} b_o d \quad (6a)$$

$$k_{cr} = \sqrt{2 \rho n_c + (\rho n_c)^2} - \rho n_c \quad (6b)$$

$$n_c = \frac{E_{refl}}{E_C} \quad (6c)$$

$$V_{cmin} = 0.132 \sqrt{f'_c} b_w d \quad (6d)$$

$$\lambda_s = \sqrt{\frac{2}{1 + 0.004d}} \leq 1.0 \quad (6e)$$

#### 3.2. Punching Shear Model Adopted in CSA/S806-12

As per CSA/S806-12 [3], the punching shear resistance is determined by selecting the lowest resistance calculated from Equations (7a)–(7c). The parameters  $\beta_c$ ,  $\lambda$ , and  $\alpha_s$  represent the ratio of the long side to the short side of the column cross-section, the concrete density factor, and the coefficient specific to the type of column (four for interior, three for edge, and two for corner columns), respectively. Similarly to the principles set forth in ACI 440, the positioning of the critical shear perimeter is standardized at a distance of

$d/2$  from the column face. Equations (7a) and (7b) are specifically devised to accommodate variations in column shape and the ratio of shear perimeter to slab depth, thus enhancing the shear strength assessment. Furthermore, a size effect is factored in for slabs with an effective depth exceeding 300 mm by incorporating a capacity adjustment with the term of  $(300/d)^{0.25}$ .

$$V_c = \left(1 + \frac{2}{\beta_c}\right) 0.028 \lambda \phi_c (E_{refl} \rho f'_c)^{1/3} b_o d \quad (7a)$$

$$V_c = \left[ \left(\frac{\alpha_s d}{b_o}\right) + 0.19 \right] 0.147 \lambda \phi_c (E_{refl} \rho f'_c)^{1/3} b_o d \quad (7b)$$

$$V_c = 0.056 \lambda \phi_c (E_{refl} \rho f'_c)^{1/3} b_o d \quad (7c)$$

### 3.3. Punching Shear Model Adopted in JSCE (2007)

The JSCE provides the punching shear resistance for two-way slabs in Equation (8) [4]. Factors  $\beta_d$ ,  $\beta_p$ , and  $\beta_r$  consider the size effect, reinforcement ratio, and elastic modulus (axial stiffness), along with the column perimeter-to-slab depth ratio ( $u/d$ ) as outlined in Equations (8b)–(8d). Equation (8e) imposes a restriction on the concrete compressive strength ( $f_{pcd}$ ), limiting it to 36 MPa. Furthermore, the factor  $\alpha$  accommodates load eccentricity (set to 1 for concentric loading), while the safety factor  $\gamma_b$  is set at 1.3. The factor  $1/\alpha$  accounts for the unbalanced moment (eccentric loading), as shown in Equation (8f), where  $e_x$  and  $e_y$  are load eccentricities in the  $x$  and  $y$  directions (mm), respectively, and  $b_x$  and  $b_y$  are critical section dimensions in the  $x$  and  $y$  directions (mm), respectively.

$$V_c = \beta_d \beta_p \beta_r \frac{f_{pcd}}{\gamma_b} \frac{1}{\alpha} b_o d \quad (8a)$$

$$\beta_d = \sqrt[4]{1/d} \leq 1.5 \quad (8b)$$

$$\beta_p = \sqrt[3]{100 \rho E_{refl} / E_s} \leq 1.5 \quad (8c)$$

$$\beta_r = 1 + [1 / (1 + 0.25 u/d)] \quad (8d)$$

$$f_{pcd} = 0.2 \sqrt{f'_c} \leq 1.2 \text{ MPa} \quad (8e)$$

$$\alpha = 1 + 1.5 \left[ (e_x + e_y) \sqrt{b_x b_y} \right] \quad (8f)$$

## 4. Punching Shear Database

An extensive literature survey of punching shear experimental programs for FRP-RC slabs performed between 1995–2019 was conducted. A total of 197 punching shear tests were collected from 41 studies (listed and cited in Appendix A Table A1 [13–40], Table A2 [23,41–49], Table A3 [50], and Table A4 [23,41,46,47]). Out of the 197 tests, 155 specimens were subjected to concentric loading and 42 specimens were subjected to eccentric loading simulating the addition of an unbalanced moment. One hundred and eighty specimens were tested without shear reinforcement and 17 were tested with shear reinforcement. Figure 3 shows the characteristics of the collected database.

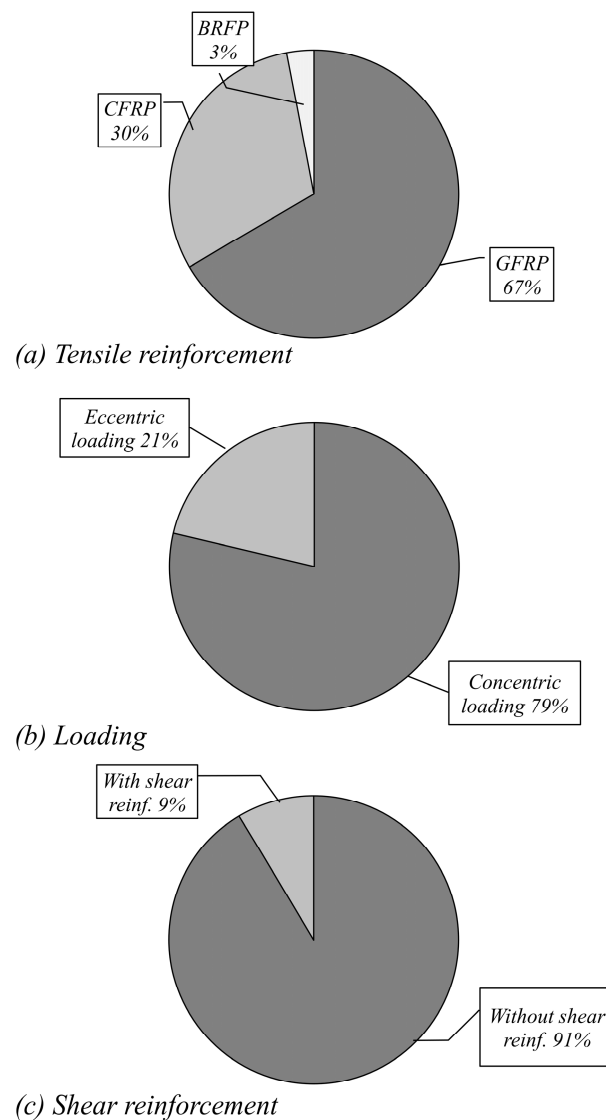


**Figure 3.** Characteristics of the surveyed database (197 specimens).

Variables collected in the database include: column and slab dimensions, slab effective depth ( $d$ ), concrete compressive strength ( $f'_c$ ), tensile reinforcement ratio ( $\rho$ ), elastic modulus for tensile reinforcement ( $E_f$ ), shear reinforcement properties (if exist), and unbalanced moment-to-shear force ( $M/V$ ). Figure 4 shows the distribution and range of  $d$ ,  $f'_c$ , and  $\rho$  in the collected database. The importance of the database in this study comes from the need for an experimental database to conduct a data-driven code evaluation, and from the size of the presented database, where the presented database is the largest database published in the literature to the authors best knowledge. With the large experimental database, different loading scenarios were evaluated, and different codes will be evaluated with the same database.

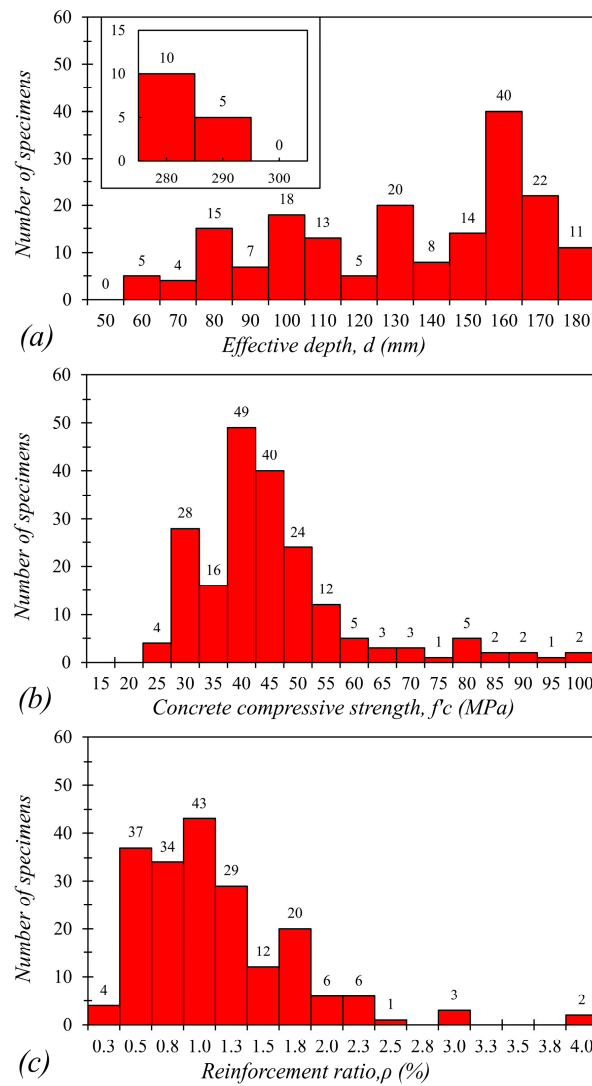


Figure 4. Distribution of design parameters in the database: (a) effective depth; (b) concrete compressive strength; (c) tensile reinforcement ratio.

### 5. Assessment of Design Provisions

For comparison reasons, the database was divided into two parts; connections without shear reinforcement (180 specimens) and connections with shear reinforcement (17 specimens). The difference between the two parts in terms of the number of specimens is due to the limited number of tests conducted with shear reinforcement. The comparison was conducted using statistical measures, including average (*Avg*), standard deviation (*SD*), coefficient of variation (*CoV*), and absolute average error (*AAE*) of the experimental-to-predicted ratios ( $V_{exp}/V_{pred}$ ). The *AAE* was calculated according to Equation (9). In addition, the number of specimens with  $V_{exp}/V_{pred} < 0.75$  is reported. In the case of eccentric load, the eccentric shear stress model mentioned in the CSA/A23.3-19 and ACI 318-19 codes (Equations (2) and (3)) was adopted to estimate the applied shear stress to connections for all design models.

$$AAE = \frac{1}{N} \sum_{i=1}^N \left| \frac{V_{pred,i} - V_{exp,i}}{V_{exp,i}} \right| \tag{9}$$

### 5.1. Assessment of Design Models for Connections without Shear Reinforcement

The  $V_{exp}/V_{pred}$  ratios for the connections without shear reinforcement in the database are plotted in Figure 5 for the ACI 440.11-22, CSA/S806-12, and the JSCE-2007 design models described in Section 4. The ratios are plotted versus the effective depth ( $d$ ), concrete compressive strength ( $f'_c$ ), reinforcement ratio ( $\rho$ ), and the FRP tensile reinforcement elastic modulus ( $E_f$ ). The  $V_{exp}/V_{pred}$  ratios are also listed in Appendix A Tables A1 and A2.

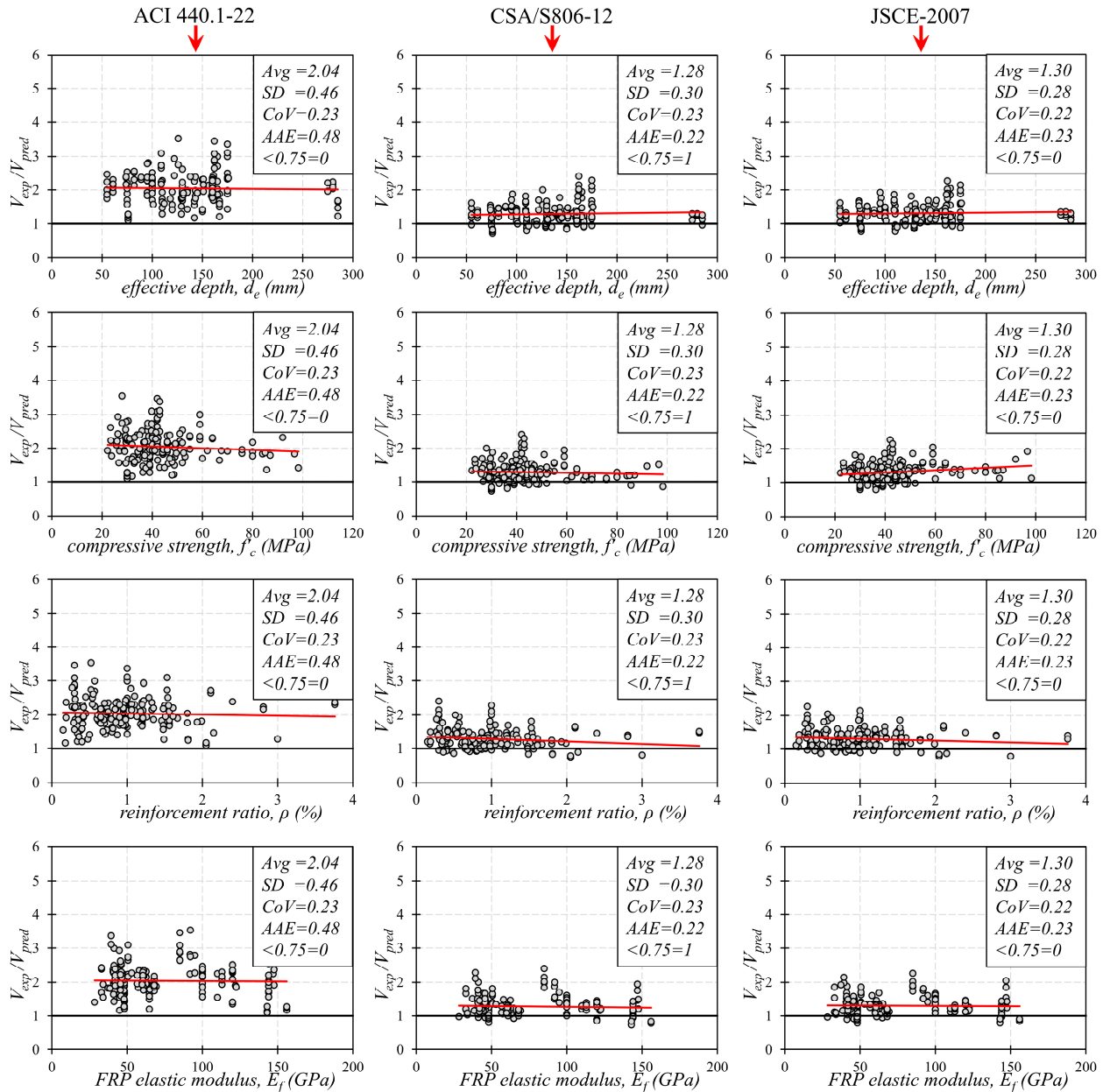


**Figure 5.** Shear strength ratio using ACI 440.11-22, CSA/S806-12, and the JSCE-2007 design models for specimens without shear reinforcement versus design parameters.

It can be noted that all models provide conservative predictions with  $Avg$  value  $V_{exp}/V_{pred}$  ratios greater than 1.0. However, the ACI 440.11-22 model results in the highest conservatism among the models, with an  $Avg.$  of 2.04 compared to 1.28 and 1.3 for the CSA/S806-12 and the JSCE-2007 models, respectively. The high conservatism of the ACI 440 model was expected as the model assumes that only the uncracked region of the slab contributes to the shear capacity. The high conservatism for the ACI 440.11-22 model results in a high  $SD$  and  $AAE$ , while the CSA/S806-12 and the JSCE-2007 models have similar

measures. However, all models result in a similar CoV of 23%. Despite the differences in statistical measures, all models result in a horizontal trendline with all variables indicating a consistent bias across the variables' ranges. This also implies that the models are applicable to the whole range of variables. Additional development in this area can be found in recent publications [51–54].

5.2. Assessment of Design Models for Connections with Shear Reinforcement

Design guidelines discussed in Section 4 do not include provisions for punching shear with FRP shear reinforcement. However, the ACI 318-19 design standard and researchers' studies recommend reducing the concrete contribution ( $V_c$ ) to half when shear reinforcement exists. This led to Equations (10) and (11) for ACI 440.11-22 and CSA/S806-12, respectively. No recommendations for the JSCE-2007 were found. The shear reinforcement contribution ( $V_f$ ) is calculated according to Equation (5), where the stress in shear reinforcement ( $f_{fv}$ ) is taken as  $f_{fv} = 0.005 E_{vf}$ , as recommended for beam shear reinforcement the design standards. Similarly to the previous section, the  $V_{exp}/V_{pred}$  ratios for connections with shear reinforcement in the database are plotted in Figure 6 and listed in Appendix A Tables A3 and A4. The ratios are plotted versus the shear reinforcement area ( $A_{vf}$ ) and elastic modulus ( $E_{vf}$ ).

$$V_c = 0.4 \lambda_s \sqrt{f'_c} k_{cr} b_o d \tag{10}$$

$$V_c = 0.028 \lambda \phi_c (E_{reft} \rho f'_c)^{1/3} b_o d \tag{11}$$

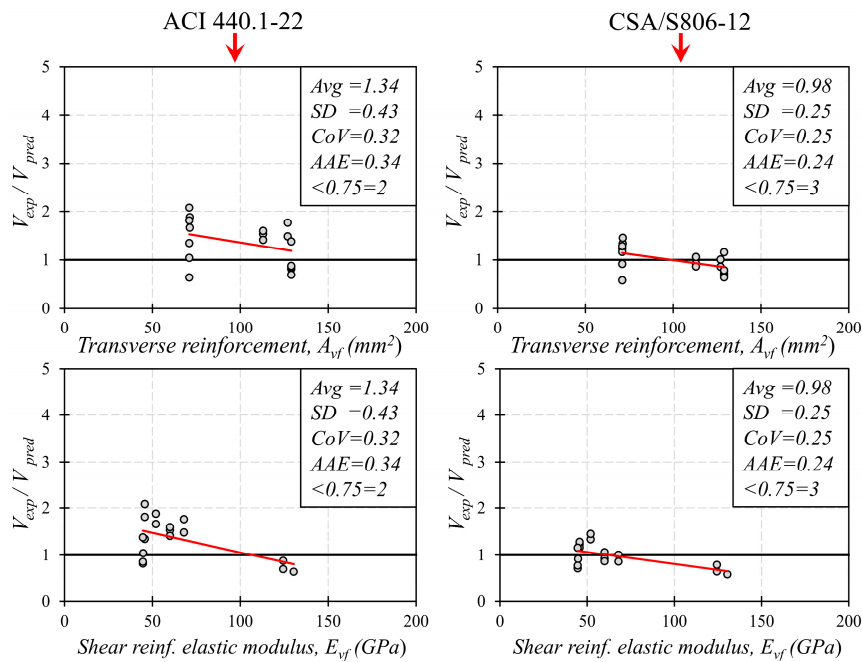


Figure 6. Shear strength ratio using ACI 440.11-22 and CSA/S806-12 design models for specimens with FRP shear reinforcement versus design parameters.

The statistical measures indicate that the ACI 440.11-22 model results in conservative predictions with an Avg of 1.34 for the  $V_{exp}/V_{pred}$  ratios. The CSA/S806-12 model results in a slightly unconservative estimate with Avg of 0.98 for the  $V_{exp}/V_{pred}$  ratios. However, the ACI 440 results in higher variability, as indicated by the 32% CoV compared to 25% for the CSA/S806-12 model. On the other hand, the trendlines indicate downward trends with respect to the variables for both models. By examining the  $V_{exp}/V_{pred}$  ratios with respect to  $E_{vf}$ , it can be noted that all specimens with  $E_{vf} > 100$  GPa resulted in  $V_{exp}/V_{pred}$  ratios less than 1.0. This indicates that the proposed procedures (Equations (10) and (11))

are not applicable for CFRP shear reinforcement. In addition, it should be noted that these specimens are from the same study. Further evaluation is required when additional experimental data are available.

## 6. Summary and Conclusions

Several design standards have been developed in the last two decades to estimate the punching capacity of two-way FRP-RC slabs, including the recently published ACI 440.11-22, CSA/S806-12, and JSCE-2007. These models were empirically or semi-empirically derived and calibrated with different databases. Additionally, these standards do not have provisions for connections with shear reinforcement. Therefore, a reliable worldwide database for developing or assessing the applicability of such provisions with test results is vital. This study presents a worldwide and up-to-date database for punching shear of FRP-RC slabs. The database includes 197 tested connections comprising a wide range of materials and cross-sectional properties. The database was used to evaluate the accuracy of the mentioned standards in predicting the punching shear capacity. The following conclusions can be drawn from the study:

1. The surveyed worldwide database comprised 197 punching shear tests for FRP-RC column–slab connections. In the database, 67% of the specimens were reinforced with GFRP, followed by CFRP (30%) and BFRP (3%). The percentage of specimens subject to an unbalanced moment (eccentric loading) was 21% compared to 79% of the specimens subjected to concentric loading. Moreover, less than 10% of the specimens were reinforced with FRP shear reinforcement. The database covered a wide range of material and cross-sectional properties.
2. For connections without shear reinforcement, the ACI 440.11-12 model resulted in the highest conservatism among the models, with an *Avg.* of 2.04 compared to 1.28 and 1.3 for the CSA/S806-12 and the JSCE-2007 models, respectively. The high conservatism of the ACI 440 model is due to the assumption that only the uncracked region of the slab contributes to the shear capacity. The high conservatism for the ACI 440.11-22 model resulted in a high *SD* and *AAE*, while the CSA/S806-12 and the JSCE-2007 models had similar measures. However, all models resulted in a similar *CoV* of 23%. All models resulted in a horizontal trendline with all variables indicating a consistent prediction accuracy across variables' ranges.
3. For connections with FRP shear reinforcement, the statistical measures indicate that the ACI 440.11-22 model resulted in conservative predictions with an *Avg* of 1.34 for the  $V_{exp}/V_{pred}$  ratios. The CSA/S806-12 model resulted in a slightly unconservative estimate with *Avg* of 0.98 for the  $V_{exp}/V_{pred}$  ratios. However, the ACI 440 resulted in higher variability, as indicated by the 32% *CoV* compared to 25% for the CSA/S806-12 model. On the other hand, the trendlines indicate downward trends with respect to the variables for both models.
4. By examining the  $V_{exp}/V_{pred}$  ratios with respect to  $E_{vf}$ , it can be noted that all specimens with  $E_{vf} > 100$  GPa resulted in  $V_{exp}/V_{pred}$  ratios less than 1.0. This indicates that the proposed procedures (Equations (10) and (11)) are not applicable for CFRP shear reinforcement. Further evaluation is required when additional experimental data is available.
5. In future work, it is recommended that researchers focus on connections with FRP shear reinforcement in terms of experimental and analytical work due to the limited data available in this area.

**Author Contributions:** Conceptualization Y.A., A.T. and A.A. (Ahmad Aldiabat); methodology, Y.A., A.T. and A.A. (Abdullah Alghossoon); validation, A.A. (Abdullah Alghossoon), R.A., Y.A. and A.A. (Ahmad Aldiabat); formal analysis, A.T. and A.A. (Ahmad Aldiabat); investigation, Y.A.; resources, A.T.; data curation, A.A. (Ahmad Aldiabat); writing—original draft preparation, Y.A., A.T. and A.A. (Ahmad Aldiabat); writing—review and editing, R.A. and A.A. (Abdullah Alghossoon); visualization, A.T.; supervision, Y.A. All authors have read and agreed to the published version of the manuscript.

**Funding:** This research received no external funding.

**Data Availability Statement:** Data used in the analysis can be found in Appendix A.

**Conflicts of Interest:** The authors declare no conflict of interest.

### Appendix A

**Table A1.** Connections under concentric loading without shear reinforcement.

Specimen	Location	Type	$L_1$ (mm)	$L_2$ (mm)	$C_1$ (mm)	$C_2$ (mm)	$d$ (mm)	$f'_c$ (MPa)	$E_f$ (GPa)	$\rho_f$	$V_{exp}$ (kN)	$V_{exp}/V_{Pred}$		
												ACI 440.1R-22	CSA/S806-12	JSCE (1997)
<b>El-Ghandour et al. (2003) [13]</b>														
SG1	interior	GFRP	2000	2000	200	200	142	32	45	0.18	170	1.16	1.13	1.06
SC1	interior	CFRP	2000	2000	200	200	142	32.8	110	0.15	229	1.55	1.2	1.11
SG2	interior	GFRP	2000	2000	200	200	142	46.4	45	0.38	271	1.54	1.25	1.24
SG3	interior	GFRP	2000	2000	200	200	142	30.4	45	0.38	237	1.66	1.25	1.18
SC2	interior	CFRP	2000	2000	200	200	142	29.6	110	0.35	317	2.2	1.29	1.22
<b>T. Hassan et al. (2000) [14]</b>														
1	Interior	CFRP	1800	3000	575	225	165	59	147	0.57	1000	2.25	1.46	1.54
2	Interior	CFRP	1800	3000	575	225	165	59	147	0.57	1200	2.7	1.75	1.85
3	Interior	CFRP	1800	3000	575	225	165	59	147	0.57	1328	2.3	1.94	2.04
<b>Rahman et al. (2000) [15]</b>														
1	interior	CFRP	2000	2500	250	150	162	42	85	0.3	622	3.08	2.15	2.02
2	interior	CFRP	2000	2500	250	150	162	42	85	0.3	698	3.46	2.41	2.27
3	interior	CFRP	2000	2500	250	150	162	42	85	0.3	575	2.85	1.99	1.87
4	interior	CFRP	2000	2500	250	150	162	42	85	0.3	534	2.64	1.84	1.74
5	interior	CFRP	2000	2500	250	150	162	42	85	0.3	584	2.89	2.02	1.9
<b>H.J. Louka (1999) [16]</b>														
1	interior	GFRP	3000	1800	575	225	175	43	41.3	1	500	1.43	0.95	0.9
2	interior	GFRP	3000	1800	575	225	175	43	41.3	1	1050	2.99	2	1.88
3	interior	GFRP	3000	1800	575	225	175	43	41.3	1	875	2.5	1.67	1.57
4	interior	GFRP	3000	1800	575	225	175	43	39.3	1	1090	3.11	2.11	1.98
5	interior	GFRP	3000	1800	575	225	175	43	39.3	1	1180	3.37	2.29	2.15
c1	interior	CFRP	3000	1800	575	225	175	55	100	1	1180	2.32	1.54	1.57
c2	interior	CFRP	3000	1800	575	225	175	55	100	1	1000	1.97	1.31	1.33
c3	interior	CFRP	3000	1800	575	225	175	55	100	1	1200	2.36	1.57	1.6
<b>K. Bouguerra et al. (2011) [17]</b>														
G-200-N	interior	GFRP	3000	2500	600	250	165	49.1	44.5	1.2	732	2.02	1.23	1.27
G-175-N	interior	GFRP	3000	2500	600	250	143	35.2	41.6	1.2	484	1.82	1.12	1.06
G-150-N	interior	GFRP	3000	2500	600	250	118	35.2	41.6	1.2	362	1.73	1.06	1.04
G-175-H	interior	GFRP	3000	2500	600	250	143	46.8	41.6	1.2	704	2.38	1.48	1.53
G-175-N-0.7	interior	GFRP	3000	2500	600	250	143	53.1	41.6	0.7	549	1.75	1.32	1.43
G-175-N-0.35	interior	GFRP	3000	2500	600	250	143	35.1	41	0.35	506	1.98	1.77	1.68
C-175-N	interior	CFRP	3000	2500	600	250	145	40.3	122	0.4	530	1.9	1.16	1.14
<b>Dulude et al. (2013) [18]</b>														
G(0.7)30/20	interior	GFRP	2500	2500	300	300	130	34.3	48.2	0.71	329	1.89	1.16	1.16
G(1.6)30/20	interior	GFRP	2500	2500	300	300	130	38.6	48.1	1.56	431	1.92	1.12	1.14
G(0.7)45/20	interior	GFRP	2500	2500	450	450	135	44.9	48.2	0.71	400	1.42	0.91	1.03
G(1.6)45/20	interior	GFRP	2500	2500	450	450	130	32.4	48.1	1.56	504	1.74	1.03	1.11
G(0.3)30/35	interior	GFRP	2500	2500	300	300	285	34.3	48.2	0.34	825	1.64	1.24	1.19
G(0.7)30/35	interior	GFRP	2500	2500	300	300	280	39.4	48.1	0.73	1071	2.04	1.23	1.2
G(0.3)45/35	interior	GFRP	2500	2500	450	450	285	48.6	48.2	0.34	911	1.21	0.97	1.1
G(0.7)45/35	interior	GFRP	2500	2500	450	450	280	29.6	48.1	0.73	1248	2.17	1.25	1.32

Table A1. Cont.

Specimen	Location	Type	$L_1$ (mm)	$L_2$ (mm)	$C_1$ (mm)	$C_2$ (mm)	$d$ (mm)	$f_c$ (MPa)	$E_f$ (GPa)	$\rho_f$	$V_{exp}$ (kN)	$V_{exp}/V_{Pred}$		
												ACI 440.1R-22	CSA/S806-12	JSCE (1997)
<b>Hassan et al. (2013b) [19]</b>														
G(0.7)30/20-B	interior	GFRP	2500	2500	300	300	135	39	48.2	0.71	386	1.98	1.24	1.25
G(1.6)30/20-B	interior	GFRP	2500	2500	300	300	130	32	48.1	1.56	451	2.11	1.25	1.27
G(1.6)45/20-B	interior	GFRP	2500	2500	450	450	130	39	48.1	1.56	511	1.68	0.98	1.07
G(0.3)30/35-B	interior	GFRP	2500	2500	300	300	285	39	48.2	0.34	782	1.46	1.13	1.11
G(0.7)30/35-B-1	interior	GFRP	2500	2500	300	300	280	30	48.1	0.73	1027	2.24	1.29	1.26
G(0.7)30/35-B-2	interior	GFRP	2500	2500	300	300	280	47	48.1	0.73	1195	2.08	1.29	1.34
G(0.3)45/35-B	interior	GFRP	2500	2500	450	450	285	32	48.2	0.34	1020	1.68	1.25	1.3
<b>Matthys, S., and L. Taerwe. (2000) [6]</b>														
C1	interior	CFRP	1000	1000	133 *	133 *	96	30.4	91.8	0.27	181	2.81	1.87	1.76
C1' interior	interior	CFRP	1000	1000	203 *	203 *	96	30.4	91.8	0.27	189	2.25	1.5	1.51
C2	interior	CFRP	1000	1000	133 *	133 *	95	29.6	95	1.05	255	2.78	1.7	1.61
C2'	interior	CFRP	1000	1000	203 *	203 *	95	29.6	95	1.05	273	2.28	1.39	1.41
C3	interior	CFRP	1000	1000	133 *	133 *	126	28	92	0.52	347	3.53	2	1.81
C3'	interior	CFRP	1000	1000	203 *	203 *	126	28	92	0.52	343	2.75	1.56	1.52
CS	interior	CFRP	1000	1000	133 *	133 *	95	27	147.6	0.19	142	2.37	1.49	1.43
CS'	interior	CFRP	1000	1000	203 *	203 *	95	27	147.6	0.19	150	1.92	1.2	1.24
H1	interior	(C&G)	1000	1000	133 *	133 *	95	96.7	37.3	0.62	207	1.83	1.51	1.92
H2	interior	(C&G)	1000	1000	133 *	133 *	89	29.3	40.7	3.76	231	2.31	1.47	1.4
H2'	interior	(C&G)	1000	1000	71 *	71 *	89	29.3	40.7	3.76	171	2.38	1.51	1.3
H3	interior	(C&G)	1000	1000	133 *	133 *	122	26.3	44.8	1.22	237	2.42	1.4	1.29
H3'	interior	(C&G)	1000	1000	71 *	71 *	122	26.3	44.8	1.22	217	2.93	1.69	1.41
<b>Joo-Ha Lee et al. (2009) [20]</b>														
GFU1	interior	GFRP	2300	2300	225	225	110	36.3	48.2	1.18	222	1.72	0.98	0.96
GFB2	interior	GFRP	2300	2300	225	225	110	36.3	48.2	2.15	246	1.46	0.89	0.87
GFB3	interior	GFRP	2300	2300	225	225	110	36.3	48.2	3	248	1.28	0.8	0.78
<b>Hemzah et al. (2019) [21]</b>														
C-F-S-10-4	interior	CFRP	600	600	88.6 *	88.6 *	75	51	144	0.3	103	2.21	1.34	1.33
C-F-S-10-6	interior	CFRP	600	600	88.6 *	88.6 *	75	52	144	0.45	127.3	2.53	1.43	1.44
S-F-D-10-4	interior	CFRP	600	600	100	100	75	46	144	0.6	111.5	1.89	1.11	1.09
S-F-D-10-6	interior	CFRP	600	600	100	100	75	60	144	0.9	128.7	1.69	1.03	1.1
S-F-S-10-4	interior	CFRP	600	600	100	100	75	52	144	0.3	78.65	1.56	0.95	0.97
S-F-S-10-6	interior	CFRP	600	600	100	100	75	48	144	0.45	107.25	2.04	1.16	1.16
S-F-S-7.5-4	interior	CFRP	600	600	100	100	55	49	144	0.41	57.2	1.74	0.98	1.03
S-F-S-7.5-6	interior	CFRP	600	600	100	100	55	49	144	0.61	78.65	2	1.18	1.24
<b>Elgabbas et al. (2016) [22]</b>														
S2-B	interior	BFRP	3000	2000	600	250	167	48.8	64.8	0.8	548	1.49	0.92	0.94
S3-B	interior	BFRP	3000	2000	600	250	167	42.2	69.3	0.79	665	1.88	1.15	1.12
S4-B	interior	BFRP	3000	2000	600	250	167	42.2	64.8	0.8	566	1.64	1	0.97
S5-B	interior	BFRP	3000	2000	600	250	167	47.9	64.8	1.2	716	1.67	1.06	1.07
S6-B	interior	BFRP	3000	2000	600	250	167	47.9	64.8	0.4	575.8	1.58	1.22	1.25
S7-B	interior	BFRP	3000	2000	600	250	167	47.9	64.8	0.4	436.4	1.2	0.93	0.94
<b>Gouda and El-Salakawy (2016b) [23]</b>														
G-00-XX	interior	GFRP	2800	2800	300	300	160	38	68	0.65	421	1.75	1	0.97
<b>Nguyen-Minh and Rovňák (2013) [24]</b>														
GSL-PUNC-0.4	interior	GFRP	2200	2200	200	200	129	39	48	0.48	180	1.28	0.91	0.87
GSL-PUNC-0.6	interior	GFRP	2200	2200	200	200	129	39	48	0.68	212	1.51	0.96	0.91
GSL-PUNC-0.8	interior	GFRP	2200	2200	200	200	129	39	48	0.92	244	1.73	0.99	0.95

Table A1. Cont.

Specimen	Location	Type	$L_1$ (mm)	$L_2$ (mm)	$C_1$ (mm)	$C_2$ (mm)	$d$ (mm)	$f'_c$ (MPa)	$E_f$ (GPa)	$\rho_f$	$V_{exp}$ (kN)	$V_{exp}/V_{Pred}$		
												ACI 440.1R-22	CSA/S806-12	JSCE (1997)
<b>El-Tom_Ehab (2007) [25]</b>														
1	interior	GFRP	1900	1900	250	250	110	66.8	41	1	282	1.64	1.05	1.28
2	interior	GFRP	1900	1900	250	250	110	62	41	1.2	319	1.93	1.15	1.37
3	interior	GFRP	1900	1900	250	250	110	64	41	1.5	384	2.28	1.27	1.53
4	interior	GFRP	1900	1900	250	250	150	64	41	1.2	589	2.31	1.39	1.58
5	interior	GFRP	1900	1900	250	250	145	70.1	41	1.2	487	1.91	1.17	1.38
6	interior	GFRP	1900	1900	250	250	135	67.6	41	1.2	437	1.92	1.17	1.38
<b>Zaghloul et al. (2014) [26]</b>														
F1	interior	GFRP	1500	1500	200	200	82	37.4	46	1.1	165	2.13	1.2	1.21
F2	interior	GFRP	1500	1500	200	200	112	33	45.87	0.81	170	1.59	0.94	0.91
F3	interior	GFRP	1500	1500	200	200	82	38.2	45.9	1.29	210	2.52	1.43	1.47
F4	interior	GFRP	1500	1500	200	200	82	39.7	46.1	1.54	230	2.51	1.46	1.51
F5	interior	GFRP	1500	1500	200	200	82	30	46.1	1.1	168	2.31	1.31	1.35
F6	interior	GFRP	1500	1500	200	200	82	29.4	46.1	1.1	185	2.55	1.45	1.51
<b>D.A. Jacobson et al. (2005) [27]</b>														
1	interior	GFRP	2300	2000	635	250	161	38	33	0.98	537	1.69	1.2	1.11
2	interior	GFRP	2300	2000	635	250	161	37	33	0.98	536	1.71	1.2	1.11
3	interior	GFRP	2300	2000	635	250	161	37	33	0.95	531	1.69	1.21	1.11
7	interior	GFRP	4300	2000	635	250	161	34	33	0.98	721	2.39	1.67	1.54
8	interior	GFRP	4300	2000	635	250	161	51	33	0.98	897	2.43	1.81	1.86
<b>Carlos Ospina et al. (2003) [28]</b>														
GFR-1	Interior	GFRP	2150	2150	250	250	120	29.5	34	0.73	199	1.55	1.03	1.04
GFR-2	Interior	GFRP	2150	2150	250	250	120	28.9	34	1.26	249	1.94	1.08	1.1
NEF-1	Interior	GFRP	2150	2150	250	250	120	37.5	28.4	0.87	203	1.4	0.97	0.96
<b>N. Banthia et al. (1995) [29]</b>														
1	Interior	CFRP	600	600	100	100	55	41	100	0.31	65	2.24	1.46	1.46
2	Interior	CFRP	600	600	100	100	55	52.5	100	0.31	61	1.86	1.26	1.37
3	Interior	CFRP	600	600	100	100	55	41.5	100	0.31	72	2.47	1.61	1.61
<b>El-Gamal et al. (2005) [30]</b>														
G-S1	interior	GFRP	3000	2500	600	250	159	49.6	44.6	1	740	2.13	1.38	1.43
G-S2	interior	GFRP	3000	2500	600	250	159	44.3	38.5	1.99	712	1.82	1.15	1.15
G-S3	interior	GFRP	3000	2500	600	250	156	49.2	46.5	1.21	732	2.14	1.3	1.35
C-S1	interior	CFRP	3000	2500	600	250	165	49.6	122.5	0.35	674	1.85	1.22	1.26
C-S2	interior	CFRP	3000	2500	600	250	165	44.3	122.5	0.69	799	1.86	1.19	1.19
<b>L. Nguyen-Minh and M. Rovnak (2013) [24]</b>														
GSL-PUNC-0.4	interior	GFRP	2200	2200	200	200	129	39	48	0.48	180	1.28	0.91	0.87
GSL-PUNC-0.5	interior	GFRP	2200	2200	200	200	129	39	48	0.68	212	1.51	0.96	0.91
GSL-PUNC-0.6	interior	GFRP	2200	2200	200	200	129	39	48	0.92	248	1.76	1.01	0.96
<b>S.H. Ahmad et al. (1994) [31]</b>														
CFRC-SN1	interior	CFRP	690	690	75	75	61	42.4	113	0.95	92.5	2.31	1.39	1.32
CFRC-SN2	interior	CFRP	690	690	75	75	61	44.6	113	0.95	78.8	1.94	1.17	1.12
CFRC-SN3	interior	CFRP	690	690	100	100	61	39	113	0.95	96	2.07	1.26	1.21
CFRC-SN4	interior	CFRP	690	690	100	100	61	36.6	113	0.95	99	2.17	1.32	1.25
<b>S. El-Gamal et al. (2007) [32]</b>														
G-S4	interior	GFRP	3000	2500	600	250	175	44.1	44.6	1.2	707	1.88	1.14	1.12
G-S5	interior	GFRP	3000	2500	600	250	175	44.1	43.4	1.2	735	1.98	1.2	1.18

Table A1. Cont.

Specimen	Location	Type	$L_1$ (mm)	$L_2$ (mm)	$C_1$ (mm)	$C_2$ (mm)	$d$ (mm)	$f'_c$ (MPa)	$E_f$ (GPa)	$\rho_f$	$V_{exp}$ (kN)	$V_{exp}/V_{Pred}$		
												ACI 440.1R-22	CSA/S806-12	JSCE (1997)
<b>AlHamaydeh and M. Orabi (2021) [33]</b>														
0F-60S	interior	GFRP	2000	2000	250	250	109	38	50.6	2.81	463	2.24	1.4	1.41
0F-80S	interior	GFRP	2000	2000	250	250	109	38.2	50.6	2.11	486	2.65	1.61	1.63
0F-110S	interior	GFRP	2000	2000	250	250	109	38.2	50.6	1.53	436	2.74	1.61	1.63
1.25F-60S	interior	GFRP	2000	2000	250	250	109	39.8	50.6	2.81	455	2.17	1.35	1.39
1.25F-80S	interior	GFRP	2000	2000	250	250	109	39.8	50.6	2.11	506	2.73	1.65	1.7
1.25F-110S	interior	GFRP	2000	2000	250	250	109	39.8	50.6	1.53	498	3.09	1.81	1.86
<b>Q. Zhang et al. (2005) [34]</b>														
CS1	interior	CFRP	1900	1900	250	250	100	31	120	0.41	251	2.29	1.29	1.33
CS2	interior	CFRP	1900	1900	250	250	100	33	120	0.54	293	2.32	1.35	1.38
CS3	interior	CFRP	1900	1900	250	250	100	25.7	120	0.75	285	2.09	1.28	1.36
CSHD1	interior	CFRP	1900	1900	250	250	100	35.9	120	0.54	325	2.51	1.45	1.46
CSHD2	interior	CFRP	1900	1900	250	250	100	38.6	120	0.75	360	2.36	1.41	1.45
CSHS1	interior	CFRP	1900	1900	250	250	150	85.6	120	0.36	399	1.35	0.89	1.12
CHSHS2	interior	CFRP	1900	1900	250	250	150	98.3	120	0.5	446	1.41	0.85	1.12
<b>Bank L. and Xi Z. (1995) [35]</b>														
1	interior	CFRP	1800	1500	250	250	76	30	143	2.05	186	1.14	0.75	0.82
2	interior	CFRP	1800	1500	250	250	76	30	143	2.05	179	1.09	0.73	0.78
3	interior	CFRP	1800	1500	250	250	76	30	143	1.81	199	1.28	0.84	0.91
4	interior	CFRP	1800	1500	250	250	76	30	156	2.05	198	1.17	0.78	0.84
5	interior	CFRP	1800	1500	250	250	76	30	156	1.81	201	1.25	0.82	0.89
6	interior	CFRP	1800	1500	250	250	76	30	156	1.49	190	1.27	0.83	0.9
<b>A. Hussein et al. (2004) [36]</b>														
G-S1	interior	GFRP	1830	1830	250	250	100	40	42	1.18	249	2.11	1.17	1.22
G-S2	interior	GFRP	1830	1830	250	250	100	35	42	1.05	218	1.98	1.12	1.13
G-S3	interior	GFRP	1830	1830	250	250	100	29	42	1.67	240	1.9	1.12	1.17
G-S4	interior	GFRP	1830	1830	250	250	100	26	42	0.95	210	2.21	1.23	1.31
<b>H. Zhu et al. (2012) [37]</b>														
A	interior	GFRP	1500	1500	150	150	130	22.2	45.6	0.42	176	1.93	1.33	1.28
B-2	interior	GFRP	1500	1500	150	150	130	23.5	45.6	0.42	209	2.23	1.55	1.47
B-3	interior	GFRP	1500	1500	150	150	130	23.4	45.6	0.55	245	2.62	1.67	1.58
B-4	interior	GFRP	1500	1500	150	150	130	23.8	45.6	0.29	167	1.77	1.4	1.32
C	interior	GFRP	1500	1500	150	150	130	44.4	45.6	0.42	252	1.96	1.51	1.44
<b>Khanna et al. (2000) [38]</b>														
1	interior	GFRP	2000	4000	500	250	138	35	42	2.4	756	2.4	1.45	1.49
<b>Oskouei et al. (2017) [39]</b>														
NW59	interior	GFRP	800	800	250	250	176	59	58	0.7	719	2.35	1.49	1.6
<b>Hassan et al. (2013a) [40]</b>														
G(1.6)30/20-H	interior	GFRP	2500	2500	300	300	131	75.8	57.4	1.56	547	1.85	1.06	1.35
G(1.2)30/20	interior	GFRP	2500	2500	300	300	131	37.5	64.9	1.21	438	1.9	1.12	1.13
G(1.6)30/35	interior	GFRP	2500	2500	300	300	275	38.2	56.7	1.61	1492	2.21	1.29	1.25
G(1.6)30/35-H	interior	GFRP	2500	2500	300	300	275	75.8	56.7	1.61	1600	1.96	1.1	1.34

Note: \* Indicates equivalent rectangular dimensions for circular column.

**Table A2.** Connections under eccentric loading without shear reinforcement.

Specimen	Location	Type	$L_1$ (mm)	$L_2$ (mm)	$C_1$ (mm)	$C_2$ (mm)	$d$ (mm)	$f'_c$ (MPa)	$E_f$ (GPa)	$\rho_f$	$M/V$	$V_{exp}$ (kN)	$V_{exp}/V_{pred}$		
													ACI 440.1R-22	CSA/ S806-12	JSCE (1997)
<b>A.H. Hussein &amp; E. F. El-Salakawy (2018) [41]</b>															
H-1.0-XX	interior	GFRP	2800	2800	300	300	160	80	65	0.98	0.15	461	1.82	1.15	1.3
H-1.5-XX	interior	GFRP	2800	2800	300	300	160	84	65	1.46	0.15	541	1.83	1.18	1.34
H-2.0-XX	interior	GFRP	2800	2800	300	300	160	87	65	1.93	0.15	604	1.79	1.2	1.36
<b>Gouda and El-Salakawy (2016a) [42]</b>															
GN-0.65	interior	GFRP	2800	2800	300	300	160	42	68	0.65	0.15	363	1.98	1.15	1.16
GN-0.98	interior	GFRP	2800	2800	300	300	160	38	68	0.98	0.15	378	1.86	1.08	1.05
GN-1.13	interior	GFRP	2800	2800	300	300	160	39	68	1.13	0.15	425	1.95	1.15	1.13
GN-0.65	interior	GFRP	2800	2800	300	300	160	70	68	0.65	0.15	380	1.6	1.07	1.21
<b>Gouda and El-Salakawy (2016b) [23]</b>															
G-15-XX	interior	GFRP	2800	2800	300	300	160	42	68	0.65	0.15	363	1.98	1.15	1.16
G-30-XX	interior	GFRP	2800	2800	300	300	160	42	68	0.65	0.3	296	2.05	1.19	1.21
R-15-XX	interior	GFRP	2800	2800	300	300	160	40	63.1	0.65	0.15	320	1.78	1.05	1.05
<b>Zaghloul (2007) [43]</b>															
ZJF1	interior	CFRP	1500	1500	250	250	74	46	100	1.33	0.22	171	2.33	1.5	1.63
ZJF2	interior	CFRP	1500	1500	250	250	74	47	100	0.87	0.22	144	2.34	1.45	1.59
ZJF3	interior	CFRP	1500	1500	250	250	74	46	100	1.33	0.3	134	2.12	1.37	1.49
ZJF4	interior	CFRP	1500	1500	250	250	100	46	100	1.48	0.22	250	2.19	1.36	1.48
ZJF6	interior	CFRP	1500	1500	250	350	100	47	100	1.48	0.22	235	1.69	1.06	1.19
ZJF8	interior	CFRP	1500	1500	350	250	101	26.7	100	1.48	0.22	185	1.59	1.02	1.1
<b>Eladawy et al. (2020) [44]</b>															
G4(1.06)H	interior	GFRP	2500	2500	300	300	151	92	62.6	1.06	1.72	140	2.2	1.47	1.68
<b>Eladawy et al. (2019) [45]</b>															
G1	interior	GFRP	2500	2500	300	300	151	52	62.6	1.06	1.293	140	2.16	1.23	1.34
G2	interior	GFRP	2500	2500	300	300	151	46	62.6	1.51	1.33	140	1.95	1.16	1.22
G3	interior	GFRP	2500	2500	300	300	151	46	62.6	1.06	0.872	180	2.15	1.23	1.29
<b>El-Gendy and El-Salakawy (2016) [46]</b>															
RD-XX-M	edge	GFRP	2800	1550	300	300	160	41	60	0.85	0.4	191	1.98	1.11	1.11
SC-XX-L	edge	GFRP	2800	1550	300	300	160	37	61	0.85	0.2	239	1.78	1	0.97
SC-XX-M	edge	GFRP	2800	1550	300	300	160	40	61	0.85	0.4	227	2.36	1.32	1.31
SC-XX-H	edge	GFRP	2800	1550	300	300	160	37	61	0.85	0.6	159	2.18	1.23	1.19
<b>Mostafa and El-Salakawy (2018) [47]</b>															
H-0.9-XX	edge	GFRP	2800	1550	300	300	160	80	60.85	0.84	0.4	251	1.89	1.28	1.46
H-1.35-XX	edge	GFRP	2800	1550	300	300	160	85	60.85	1.35	0.4	272	1.87	1.18	1.35
H-1.8-XX	edge	GFRP	2800	1550	300	300	160	80	60.85	1.8	0.4	288	1.77	1.14	1.3
<b>El-gendy and El-Salakawy E. (2018) [48]</b>															
GSC-0.9	edge	GFRP	2800	1550	300	300	160	40	60.5	0.9	0.4	227	2.3	1.3	1.29
GSC-1.35	edge	GFRP	2800	1550	300	300	160	42	60.5	1.35	0.4	264	2.21	1.3	1.31
GSC-1.8	edge	GFRP	2800	1550	300	300	160	42	60.5	1.8	0.4	278	2.05	1.24	1.25
GRD-0.9	edge	GFRP	2800	1550	300	300	160	41	60	0.9	0.4	191	1.93	1.09	1.09
<b>Salama et al. (2019) [49]</b>															
G	edge	GFRP	2500	1350	300	300	160	41.4	53	1.55	0.31	314	2.28	1.34	1.35

**Table A3.** Connections under concentric loading with shear reinforcement.

Specimen	Location	Type	L <sub>1</sub> (mm)	L <sub>2</sub> (mm)	C <sub>1</sub> (mm)	C <sub>2</sub> (mm)	d (mm)	f <sub>c</sub> (MPa)	E <sub>f</sub> (GPa)	ρ <sub>f</sub>	A <sub>vf</sub> (mm <sup>2</sup> )	s (mm <sup>2</sup> )	n	E <sub>vf</sub> (GPa)	V <sub>exp</sub> kN	V <sub>exp</sub> /V <sub>theo</sub>	
																ACI 440.11-22	CSA/ S806-12
<b>Hassan et al. (2014) [50]</b>																	
G(1.2)200-GCS(d/2)	interior	GFRP	2500	2500	300	300	131	37.5	64.9	1.21	71	70	16	44.8	614	1.24	1.15
G(1.2)200-CCS(d/2)	interior	GFRP	2500	2500	300	300	131	37.5	64.9	1.21	71	70	8	130.4	514	0.77	0.72
G(0.3)350-GSS(d/4)	interior	GFRP	2500	2500	300	300	284	29.5	48.2	0.34	129	70	8	44.6	885	0.98	0.89
G(1.6)350-GSS(d/4)	interior	GFRP	2500	2500	300	300	280	40.2	56.7	1.61	129	70	8	44.6	1761	1.61	1.50
G(1.6)350-GBSS(d/4)	interior	GFRP	2500	2500	300	300	280	37.5	56.7	1.61	129	70	16	44.6	1869	1.02	0.96
G(1.6)350-CSS(d/4)	interior	CFRP	2500	2500	300	300	280	38.2	56.7	1.61	129	70	8	124.4	2024	0.84	0.79
G(1.6)350-CSS(d/3)	interior	CFRP	2500	2500	300	300	280	40.2	56.7	1.61	129	100	8	124.4	1886	1.05	0.98

**Table A4.** Connections under eccentric loading with shear reinforcement.

Specimen	Location	Type	L <sub>1</sub> (mm)	L <sub>2</sub> (mm)	C <sub>1</sub> (mm)	C <sub>2</sub> (mm)	d (mm)	f <sub>c</sub> MPa	E <sub>f</sub> (GPa)	ρ <sub>f</sub>	A <sub>vf</sub> (mm <sup>2</sup> )	s (mm <sup>2</sup> )	E <sub>vf</sub> (GPa)	n	M/V	V <sub>exp</sub> kN	V <sub>exp</sub> /V <sub>theo</sub>	
																	ACI 440.11-22	CSA/ S806
<b>A.H. Hussein &amp; E. F. El-Salakawy (2018) [41]</b>																		
N-1.0-S5	interior	GFRP	2800	2800	300	300	160	43	65	0.98	127	120	68	12	0.15	595	1.76	1.01
N-1.0-S6	interior	GFRP	2800	2800	300	300	160	43	65	0.98	127	120	68	12	0.15	583	1.48	0.86
N-1.0-C5	interior	GFRP	2800	2800	300	300	160	43	65	0.98	71	120	52	12	0.15	527	1.66	1.33
<b>Gouda and El-Salakawy (2016b) [23]</b>																		
R-15-75	interior	GFRP	2800	2800	300	300	160	42	63.1	0.65	113	120	60	8	0.15	385	1.11	0.92
R-15-50	interior	GFRP	2800	2800	300	300	160	42	63.1	0.65	113	80	60	8	0.15	401	0.84	0.73
<b>Mostafa and El-Salakawy (2018) [47]</b>																		
N-0.9-C6	edge	GFRP	2800	1550	300	300	160	45	61	0.85	71.3	120	52	6	0.4	253	1.88	1.45
<b>Salama et al. (2019) [49]</b>																		
G-CS-1.75d	edge	GFRP	2500	1350	300	300	160	47.6	53	1.55	71	80	45.7	12	0.31	370	2.08	1.23
G-CS-4.25d	edge	GFRP	2500	1350	300	300	160	51.3	53	1.55	71	80	45.7	12	0.3	440	1.34	1.16
G-SS-4.25d	edge	GFRP	2500	1350	300	300	160	52.5	53	1.55	71	80	45.7	12	0.3	486	1.8	1.27
<b>El-Gendy and El-Salakawy (2016) [46]</b>																		
RD-75-M	edge	GFRP	2800	1550	300	300	160	41	60.2	0.85	113	120	60	6	0.4	256	1.41	1.06

**References**

1. Tarawneh, A.N.; Dwairi, H.M.; Almasabha, G.S.; Majdalaweyh, S.A. Effect of Fiber-Reinforced Poly-mer-Compression Reinforcement in Columns Subjected to Concentric and Eccentric Loading. *ACI Struct. J.* **2021**, *118*, 187.
2. ACI-440.11-22; Building Code Requirements for Structural Concrete Reinforced with Glass Fiber-Reinforced Polymer (GFRP) Bars—CODE AND COMMENTARY, A Report by ACI Committee 440 Farmington Hills. American Concrete Institute: Indianapolis, IN, USA, 2022.
3. CSA/S806-12 (R2017); Design and Construction of Building Structures with Fibre-Reinforced Polymer. CSA (Canadian Standard Association): Toronto, ON, Canada, 2017.
4. JSCE (Japan Society of Civil Engineering). *Recommendation for Design and Construction of Concrete Structures Using Continuous Fibre Reinforcing Materials*; Concrete Engineering Series 23; JSCE: Tokyo, Japan, 2007.
5. El-Gendy, M.G.; El-Salakawy, E.F. Assessment of punching shear design models for FRP-RC slab–column connections. *J. Compos. Constr.* **2020**, *24*, 04020047. [[CrossRef](#)]
6. Matthys, S.; Taerwe, L. Concrete Slabs Reinforced with FRP Grids. II: Punching Resistance. *J. Compos. Constr.* **2000**, *4*, 154–161. [[CrossRef](#)]
7. Peng, F.; Xue, W.; Xue, W. Database evaluation of shear strength of slender fiber-reinforced polymer-reinforced concrete members. *ACI Struct. J.* **2020**, *117*, 273–281.
8. Wight, J.K.; MacGregor, J.G. *Reinforced Concrete*; Pearson Education: London, UK, 2016.

9. Vargas, D.; Lantsoght, E.O.L.; Genikomsou, A.S. Flat Slabs in Eccentric Punching Shear: Experimental Database and Code Analysis. *Buildings* **2022**, *12*, 2092. [[CrossRef](#)]
10. Tureyen, A.K.; Frosch, R.J. Concrete shear strength: Another perspective. *Struct. J.* **2003**, *100*, 609–615.
11. Ospina, C.E. Alternative model for concentric punching capacity. *Concr. Int.* **2005**, *27*, 53–57.
12. Nanni, A.; De Luca, A.; Jawaheri Zadeh, H. *FRP Reinforced Concrete Structures—Theory, Design and Practice*; CRC Press: Boca Raton, FL, USA, 2014; ISBN 9780415778824.
13. El-Ghandour, A.W.; Pilakoutas, K.; Waldron, P. Punching shear behavior of fiber reinforced polymers reinforced concrete flat slabs: Experimental study. *J. Compos. Constr.* **2003**, *7*, 258–265. [[CrossRef](#)]
14. Hassan, T.; Abdelrahman, A.; Tadros, G.; Rizkalla, S. Fibre reinforced polymer reinforcing bars for bridge decks. *Can. J. Civ. Eng.* **2000**, *27*, 839–849. [[CrossRef](#)]
15. Rahman, A.H.; Kingsley, C.Y.; Kobayashi, K. Service and ultimate load behavior of bridge deck reinforced with carbon FRP grid. *J. Compos. Constr.* **2000**, *4*, 16–23. [[CrossRef](#)]
16. Louka, H.J. Punching Behaviour of a Hybrid Reinforced Concrete Bridge Deck. Master's Thesis, University of Manitoba, Winnipeg, MB, Canada, 1999.
17. Bouguerra, K.; Ahmed, E.A.; El-Gamal, S.; Benmokrane, B. Testing of full-scale concrete bridge deck slabs reinforced with fiber-reinforced polymer (FRP) bars. *Constr. Build. Mater.* **2011**, *25*, 3956–3965. [[CrossRef](#)]
18. Dulude, C.; Hassan, M.; Ahmed, E.A.; Benmokrane, B. Punching shear behavior of flat slabs reinforced with glass fiber-reinforced polymer bars. *ACI Struct. J.* **2013**, *110*, 723. [[CrossRef](#)]
19. Hassan, M.; Ahmed, E.A.; Benmokrane, B. Punching shear strength of glass fiber-reinforced polymer reinforced concrete flat slabs. *Can. J. Civ. Eng.* **2013**, *40*, 951–960. [[CrossRef](#)]
20. Lee, J.H.; Yoon, Y.S.; Cook, W.D.; Mitchell, D. Improving punching shear behavior of glass fiber-reinforced polymer reinforced slabs. *ACI Struct. J.* **2009**, *106*, 427.
21. Hemzah, S.A.; Al-Obaidi, S.; Salim, T. Punching shear model for normal and high-strength concrete slabs reinforced with CFRP or steel bars. *Jordan J. Civ. Eng.* **2019**, *13*, 250–268.
22. Elgabbas, F.; Ahmed, E.A.; Benmokrane, B. Experimental testing of concrete bridge-deck slabs reinforced with bas-alt-FRP reinforcing bars under concentrated loads. *J. Bridge Eng.* **2016**, *21*, 04016029. [[CrossRef](#)]
23. Gouda, A.; El-Salakawy, E. Behavior of GFRP-RC interior slab-column connections with shear studs and high-moment transfer. *J. Compos. Constr.* **2016**, *20*, 04016005. [[CrossRef](#)]
24. Nguyen-Minh, L.; Rovňák, M. Punching shear resistance of interior GFRP reinforced slab-column connections. *J. Compos. Constr.* **2013**, *17*, 2–13. [[CrossRef](#)]
25. El-Tom, E. Behavior of Two-Way Slabs Reinforced with GFRP Bars. Ph.D. Thesis, Memorial University of New-Foundland, St. John's, NL, Canada, 2007.
26. Mahmoud, Z.; Salma, T. Punching behavior and strength of slab-column connection reinforced with glass fiber rebars. In Proceedings of the 7th International Conference on FRP Composites in Civil Engineering, Vancouver, BC, Canada, 20–22 August 2014; pp. 20–22.
27. Jacobson, D.A.; Bank, L.C.; Oliva, M.G.; Russell, J.S. Punching shear capacity of double layer FRP grid reinforced slabs. In Proceedings of the 7th International Conference on Fiber Reinforced Plastics for Reinforced Concrete Structures, Kansas City, Missouri, USA, 1 October 2005; pp. 857–871.
28. Ospina, C.E.; Alexander, S.D.; Cheng, J.R. Punching of two-way concrete slabs with fiber-reinforced polymer reinforcing bars or grids. *Struct. J.* **2003**, *100*, 589–598.
29. Banthia, N.; Al-Asaly, M.; Ma, S. Behavior of concrete slabs reinforced with fiber-reinforced plastic grid. *J. Mater. Civ. Eng.* **1995**, *7*, 252–257. [[CrossRef](#)]
30. El-Gamal, S.; El-Salakawy, E.; Benmokrane, B. Behavior of concrete bridge deck slabs reinforced with fiber-reinforced polymer bars under concentrated loads. *ACI Struct. J.* **2005**, *102*, 727.
31. Ahmad, S.H.; Zia, P.; Yu, T.J.; Xie, Y. Punching shear tests of slabs reinforced with 3-dimensional carbon fiber fabric. *Concr. Int.* **1994**, *16*, 36–41.
32. El-Gamal, S.; El-Salakawy, E.; Benmokrane, B. Influence of reinforcement on the behavior of concrete bridge deck slabs reinforced with FRP bars. *J. Compos. Constr.* **2007**, *11*, 449–458. [[CrossRef](#)]
33. AlHamaydeh, M.; Orabi, M.A. Punching Shear Behavior of Synthetic Fiber-Reinforced Self-Consolidating Concrete Flat Slabs with GFRP Bars. *J. Compos. Constr.* **2021**, *25*, 04021029. [[CrossRef](#)]
34. Zhang, Q.; Marzouk, H.; Hussein, A. A preliminary study of high-strength concrete two-way slabs reinforced with GFRP bars. In Proceedings of the 33rd CSCE Annual Conference: General Conference and International History Symposium, Toronto, ON, Canada, 2–4 June 2005; pp. 1–10.
35. Bank, L.C.; Xi, Z. 43 punching shear behavior of pultruded frp grating reinforced concrete slabs. In *Non-Metallic (FRP) Reinforcement for Concrete Structures: Proceedings of the Second International RILEM Symposium*; CRC Press: Boca Raton, FL, USA, 1995; Volume 29, p. 360.
36. Hussein, A.; Rashid, I.; Benmokrane, B. Two-way concrete slabs reinforced with GFRP bars. In Proceedings of the 4th International Conference on Advanced Composite Materials in Bridges and Structures, Calgary, AB, Canada, 20–23 July 2004; pp. 20–23.

37. Zhu, H.T.; Wang, Y.Z.; Li, J.Z. Plastic analysis on punching shear capacity of two-way BFRP rebar reinforced concrete slabs under central concentrated load. *J. Zhengzhou Univ. (Eng. Sci.)* **2012**, *33*, 1–5. (In Chinese)
38. Khanna, O.S.; Mufti, A.A.; Bakht, B. Experimental investigation of the role of reinforcement in the strength of con-crete deck slabs. *Can. J. Civ. Eng.* **2000**, *27*, 475–480. [[CrossRef](#)]
39. Oskouei, A.V.; Kivi, M.P.; Araghi, H.; Bazli, M. Experimental study of the punching behavior of GFRP reinforced lightweight concrete footing. *Mater. Struct.* **2017**, *50*, 256. [[CrossRef](#)]
40. Hassan, M.; Ahmed, E.; Benmokrane, B. Punching-Shear strength of normal and high-strength two-way concrete slabs reinforced with GFRP bars. *J. Compos. Constr.* **2013**, *17*, 04013003. [[CrossRef](#)]
41. Hussein, A.H.; El-Salakawy, E.F. Punching Shear Behavior of Glass Fiber-Reinforced Polymer-Reinforced Concrete Slab-Column Interior Connections. *ACI Struct. J.* **2018**, *115*, 1075–1088. [[CrossRef](#)]
42. Gouda, A.; El-Salakawy, E. Punching shear strength of GFRP-RC interior slab-column connections subjected to moment transfer. *J. Compos. Constr.* **2016**, *20*, 04015037. [[CrossRef](#)]
43. Zaghoul, A. Punching Shear Strength of Interior and Edge Column-Slab Connections in CFRP Reinforced Flat Plate Structures Transferring Shear and Moment. Ph.D. Thesis, Carleton University, Ottawa, ON, Canada, 2007.
44. Eladawy, M.; Hassan, M.; Benmokrane, B.; Ferrier, E. Lateral cyclic behavior of interior two-way concrete slab-column connections reinforced with GFRP bars. *Eng. Struct.* **2020**, *209*, 109978. [[CrossRef](#)]
45. Eladawy, M.; Hassan, M.; Benmokrane, B. Experimental Study of Interior Glass Fiber-Reinforced Poly-mer-Reinforced Concrete Slab-Column Connections under Lateral Cyclic Load. *ACI Struct. J.* **2019**, *116*, 165. [[CrossRef](#)]
46. El-Gendy, M.G.; El-Salakawy, E. Effect of shear studs and high moments on punching behavior of GFRP-RC slab-column edge connections. *J. Compos. Constr.* **2016**, *20*, 04016007. [[CrossRef](#)]
47. Mostafa, A.M.; El-Salakawy, E.F. Behavior of GFRP-RC slab-column edge connections with high-strength concrete and shear reinforcement. *J. Compos. Constr.* **2018**, *22*, 04018001. [[CrossRef](#)]
48. El-Gendy, M.G.; El-Salakawy, E. Punching shear behavior of GFRP-RC slab-column edge connections. *Spec. Publ.* **2018**, *322*, 5.1–5.20.
49. Salama, A.E.; Hassan, M.; Benmokrane, B. Effectiveness of Glass Fiber-Reinforced Polymer Stirrups as Shear Rein-forcement in Glass Fiber-Reinforced Polymer-Reinforced Concrete Edge Slab-Column Connections. *ACI Struct. J.* **2019**, *116*. [[CrossRef](#)]
50. Hassan, M.; Ahmed, E.A.; Benmokrane, B. Punching-shear design equation for two-way concrete slabs reinforced with FRP bars and stirrups. *Constr. Build. Mater.* **2014**, *66*, 522–532. [[CrossRef](#)]
51. Momani, Y.; Tarawneh, A.; Alawadi, R.; Taqieddin, Z.N.; Jweihan, Y.S.; Saleh, E. Predictive models of behavior and capacity of FRP reinforced concrete columns. *J. Appl. Eng. Sci.* **2023**, *21*, 143–156. [[CrossRef](#)]
52. Saleh, E.; Tarawneh, A.; Almasabha, G.; Momani, Y. Slenderness limit of FRP-confined rectangular concrete columns. *Structures* **2022**, *38*, 435–447. [[CrossRef](#)]
53. Saleh, E.; Alghossoon, A.; Tarawneh, A. Optimal allocation of material and slenderness limits for the rectangular concrete-filled columns. *J. Constr. Steel Res.* **2022**, *193*, 107283. [[CrossRef](#)]
54. Tarawneh, A.; Momani, Y.; Alawadi, R. Leveraging artificial intelligence for more accurate and reliable predictions of anchors shear breakout capacity in thin con-crete members. *Structures* **2021**, *32*, 1005–1014. [[CrossRef](#)]

**Disclaimer/Publisher’s Note:** The statements, opinions and data contained in all publications are solely those of the individual author(s) and contributor(s) and not of MDPI and/or the editor(s). MDPI and/or the editor(s) disclaim responsibility for any injury to people or property resulting from any ideas, methods, instructions or products referred to in the content.